frontiers | Frontiers in Lab on a Chip Technologies

TYPE Mini Review
PUBLISHED 01 February 2024
DOI 10.3389/frlct.2024.1356800

OPEN ACCESS

EDITED BY
Xiangchun Xuan,
Clemson University, United States

REVIEWED BY
Teng Zhou,
Hainan University, China

*CORRESPONDENCE
Zhigang Li,
mezli@ust.hk

RECEIVED 16 December 2023
ACCEPTED 08 January 2024
PUBLISHED 01 February 2024

CITATION
Shi D, Zhou L and Li Z (2024), Nanofluidic systems for ion transport with tunable surface charges: fabrications, characterizations, and applications.
Front. Lab. Chip. Technol. 3:1356800.
doi: 10.3389/frlct.2024.1356800

Nanofluidic systems for ion transport with tunable surface charges: fabrications, characterizations, and applications

Dachuang Shi, Le Zhou and Zhigang Li*

Department of Mechanical and Aerospace Engineering, The Hong Kong University of Science and Technology, Kowloon, Hong Kong SAR, China

Nanofluidics deals with the statics and dynamics of simple and complex fluids in systems with at least one dimension below 100 nm. Under strong nanoconfinements, flows may show diverse phenomena, which find rich applications in a variety of areas. In the past decades, nanofluidics has attracted great interest. Particularly, surface charge-governed ion transport in nanofluidic systems shows new flow fashions that cannot be observed in bulk systems and have been applied in different fields in science and engineering. These applications have motivated many efforts in developing surface charge-governed nanofluidic systems, including device fabrications and characterizations. Recent advances in nanotechnology have led to significant progress in surface modifications, which offer new opportunities for surface charge-governed nanofluidics systems. In this review, we discuss recent development of nanofluidic systems with tunable surface charges. Specifically, relevant theories, experimental approaches, and performance comparisons regarding the state-of-the-art fabrication techniques, characterization methods, and applications are presented. Finally, we provide a perspective about the possible future topics and applications for advancing nanofluidic systems with tunable surface charge properties.

KEYWORDS

nanofluidics, surface charge density, nanofabrication, characterization, ion transport

1 Introduction

Nanofluidics is a subject dealing with fluid statics and dynamics in systems with a least one dimension below 100 nm. Due to strong confinement effects at the nanoscale, flows in nanofluidic systems may exhibit unique phenomena, which are different from what can be observed in micro- and macro-systems (Rauscher and Dietrich, 2008; Schoch et al., 2008; Bocquet and Charlaix, 2010; Li, 2018; Timperman, 2019; Qian and Xuan, 2020; Li, 2022). Therefore, nanofluidics has attracted great attention in the past decades. Among various flows, ion transport at the nanoscale is a popular topic in nanofluidics (Daiguji, 2010; Han and Chen, 2020; Tao et al., 2021). Because the characteristic dimensions of nanofluidic systems is comparable to or even smaller than the Debye length, the surface charge of a nanofluidic system is of essential importance in ion transport (Stein et al., 2004; Vlassiouk et al., 2008; Ma et al., 2017). In addition to be a scientific focus, nanoscale surface charge-governed ion

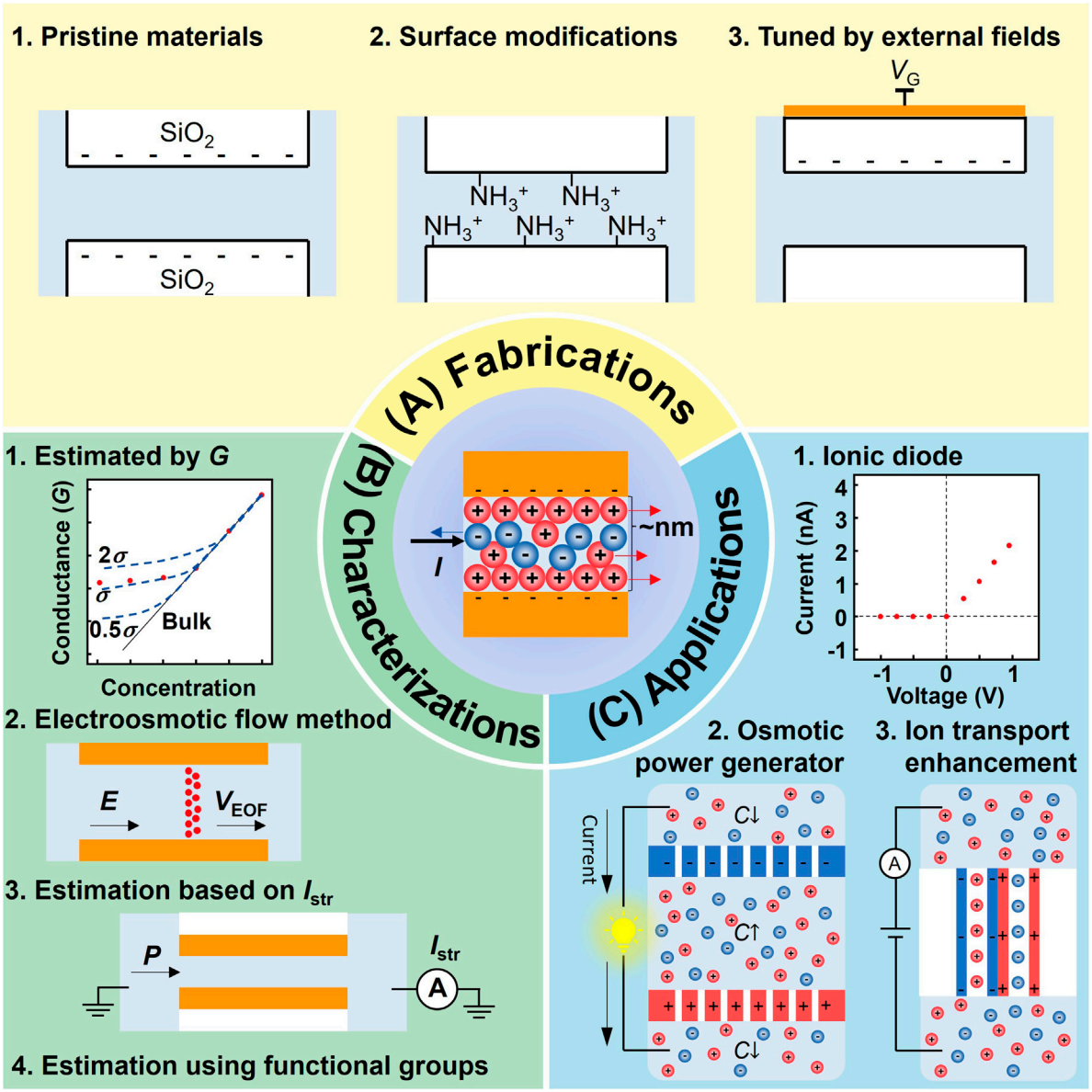

FIGURE 1
Three aspects of nanofluidic systems with tunable surface charges for ion transport. **(A)** Fabrication techniques. **(B)** Characterization methods. **(C)** Applications.

transport plays a critical role in industrial applications as it can be used in a variety of areas, including lab on a chip technologies (Fu et al., 2007; Zhou et al., 2008; Napoli et al., 2010; Utko et al., 2011; Rems et al., 2016), various sensing (Vlassiouk et al., 2009; Zhou et al., 2011; Kang et al., 2012; Sang et al., 2013; Zhao et al., 2016; Li et al., 2021; Jia et al., 2022), ionic flow regulation (Daiguji et al., 2005; Fan et al., 2005; Karnik et al., 2007; Miedema et al., 2007; Vlassiouk and Siwy, 2007; Yeh et al., 2013; Fuest et al., 2017; Li et al., 2019; Wang and Chen, 2022), energy harvesting (van der Heyden et al., 2006; Bakli and Chakraborty, 2015; Xiao et al., 2018; Gao et al., 2019; Zhou et al., 2019; Zhang et al., 2022) and storage (Daiguji et al., 2006; Pan et al., 2017; Yan et al., 2017; Jin et al., 2020; Liu et al., 2022; Si et al., 2023), to name a few. In the literature, many efforts have been made to design and fabricate nanofluidic systems with tunable surface charges. Surface charge properties of different materials have been studied and characterized. However, a review of nanofluidic systems with tunable surface charges for ion transport is lacking.

It is known that the surface charge density of a material may vary if it undergoes different fabrication processes (Stein et al., 2004). The surface charge density can also be altered through surface modifications using functional groups (Vlassiouk and Siwy, 2007) or external factors such as electric fields (Guan, 2013). These methods provide diverse options for tuning the surface charge density to regulate ion transport. A review that summarizes different methods for surface charge tunning and characterization is necessary. Furthermore, analyses and comparisons of the mechanisms for surface charge modification and the predictions of surface charges are needed.

TABLE 1 Surface charge densities of different materials under various fabrication processes.

Materials	Charge density (mC m^{-2})	Fabrication method	Refs.
Fused silica	−60	Reactive CHF_3/O_2 plasma etching	Stein et al. (2004)
Pyrex® glass	−25	Field-assisted bonding process	Schoch and Renaud (2005)
Glass substrate (bottom) and SiO_2 (cap)	−4.24	PECVD grew SiO_2	Cheng and Guo (2009)
SiO_2 (bottom) and glass (cap)	−1.5	SiO_2 was coated by thermal oxidation on Si subtract and nanochannels were made by FIB milling	Lebedev et al. (2021)
Monodispersed silica nanoparticle	−18	Stöber process	Chen et al. (2009), Ouyang et al. (2013)
Graphene (bottom) and SiO_2 (cap)	−5.5 to −4.7	Graphene was prepared by CVD. The device was fabricated by graphene transfer, etching, and bonding process	Xie et al. (2016)
Graphene (bottom) and SiO_2 (cap)	−8	Graphene was prepared by CVD. The device was fabricated by graphene transfer, etching, and bonding process	Xie et al. (2018)
Graphite	−0.02	Van der Waals (vdW) assembly	Esfandiar et al. (2017)
Single-walled carbon nanotubes (SWCNTs)	−16 to −13	SWCNTs were grown by CVD.	Pang et al. (2011)
Double-walled carbon nanotubes (DWCNTs)	−203.8 to −1.2	DWCNTs were grown by CVD.	Cui et al. (2023a)
Hexagonal boron nitride (hBN)	−0.12	Van der Waals (vdW) assembly	Esfandiar et al. (2017)
MoS_2	−0.3	Van der Waals (vdW) assembly	Esfandiar et al. (2017)
Silicon nitride (SiN_x, substrate) and black phosphorus (BP, covering layer)	−4	Van der Waals (vdW) assembly	Cui et al. (2023b)
Boron nitride nanotubes (BNNTs)	−1000 to −100	*In situ* SEM insertion	Siria et al. (2013)
PET nanopores	−240	Track-etch method	Siwy et al. (2005)
PET nanopores	−20 to −10	Track-etch method	Xue et al. (2009)
Graphene oxide (GO) nanosheet membrane	−20.1 to −0.12	GO membrane was mounted on a SiN_x layer on a Si substrate chip	Hong et al. (2017)
Boron nitride (BN) membrane	−840	BN nanosheets were synthesized by a one-step mechano-chemical process, and the membrane was prepared by vacuum filtration	Qin et al. (2017)
MXene $Ti_3C_2T_x$ membrane	−100	MXene $Ti_3C_2T_x$ was prepared by selective aluminum layer etching, and the membrane was made by filtering	Hong et al. (2019)
Metal-organic framework (MOF), UiO-66-COOH membrane	−800	Nanoconfined interfacial strategy	Lu et al. (2021)
Al_2O_3	2.10	E-beam evaporation	Cheng and Guo (2009)
MgO	1.36	E-beam evaporation	Cheng (2008)
NiO	3.77	E-beam evaporation and oxidation	Cheng (2008)

In this work, we provide a mini review of nanofluidic systems with tunable surface charges for ion transport. Three aspects of the fluidic systems: fabrications, characterizations, and applications, are discussed, as shown in Figure 1. In Section 2, three methods for tuning surface charges, which use pristine materials, achieve charge variation through surface modifications, and utilize external fields, are introduced. In Section 3, four primary approaches for characterizing the surface charge density using ionic conductance, electroosmotic flow velocity (V_{EOF}), streaming current (I_{str}), and density of functional groups, are discussed. Enabled by various fabrication and characterization technologies, a variety of applications are summarized in Section 4. The applications include ionic diodes, osmotic power generators, and ion transport enhancement. Finally, a perspective about the future development of nanofluidic systems with tunable surface charge properties for ion transport is provided in Section 5.

2 Fabrications of nanofluidic systems with tunable surface charges

2.1 Surface charge tuning using pristine materials

Many pristine surfaces can carry charges during a fabrication process and the charge polarity and density depend on the specific

method for creating the surface of flow channels and the properties of the surface material, as will be discussed later. As the surface charge of pristine surfaces does not require chemical modifications, nanofluidic systems with pristine surfaces have been widely used to study surface charge-governed ionic flows. Table 1 lists various materials and the surface charge densities generated by different fabrication methods.

Silicon-dioxide (SiO_2)-based materials have been used in early studies that revealed the effects of surface charges on the ion transport in nanochannels. In most of those work, nanochannels were fabricated on a fused silica substrate by reactive CHF_3/O_2 plasma etching. The silica substrate was then bonded with a fused silica cover. Eventually, the nanofluidic system was accomplished by connecting the nanochannels with two micro reservoirs. The surface charge density of nanoslits fabricated through this method was reported to be -60 mC m^{-2} (Stein et al., 2004). A similar configuration consisting a substrate with etched structures and a cover plate was achieved by using two pieces of Pyrex® glass. Schoch et al. fabricated a nanoslit array on a Pyrex® glass substrate, which was enclosed by another piece of Pyrex® glass through a field-assisted bonding process. The fluidic system showed a surface charge density of -25 mC m^{-2} (Schoch and Renaud, 2005). Besides commercially available SiO_2-based materials, laboratory-made SiO_2 layers can also be used for nanofluidic system fabrications. Cheng et al. developed a nanoslit system by utilizing a glass substrate as the bottom surface and growing a SiO_2 layer on the substrate through a plasma-enhanced chemical vapor deposition (PECVD) method. The as-prepared nanoslits showed a surface charge density of -4.24 mC m^{-2} (Cheng and Guo, 2009).

SiO_2 layers can also be grown on substrates through thermal oxidation. Lebedev et al. first grew a SiO_2 layer on a Si substrate through thermal oxidation, which was followed by engraving nanometer-deep trenches in the SiO_2 layer by focusing ion beam (FIB) milling. Then, the substrate was encapsulated by a glass cover and a nanoslit array was achieved. The nanoslits made using this method displayed a surface charge density of -1.5 mC m^{-2} (Lebedev et al., 2021). Special nanochannels formed by assembling silica nanoparticles in micropores has been demonstrated and the resulting nanochannels were showed to have a surface charge density of -18 mC m^{-2}. Pristine carbon-based materials also display a negatively charged surface. Xie et al. proposed a two-dimensional (2D) nanofluidic system consisting of a graphene layer on the bottom surface of nanochannels and a glass cover. The system showed surface charge densities ranging from -5.5 to -4.7 mC m^{-2} (Xie et al., 2016). A similar nanofluidic system with nanoslits partially covered by graphene was also fabricated, and the surface charge density was determined as -8 mC m^{-2} (Xie et al., 2018). However, graphite, consisting of several graphene layers, demonstrates a relatively weak surface charge density. Esfandiar et al. fabricated graphite nanoconduits by the van der Waals (vdW) assembly, which demonstrated a surface charge density of -0.02 mC m^{-2}. The low surface charge density was attributed to the spotless fabrication environment and the defect-free graphite (Esfandiar et al., 2017). Using single-walled and double-walled carbon nanotubes grown by chemical vapor deposition (CVD), one-dimensional (1D) nanofluidic systems were fabricated. The performance of these systems indicated that the surface charge densities for single-walled and double-walled carbon nanotubes were -16 to -13 and -203.8 to -1.2 mC m^{-2} respectively (Pang et al., 2011; Cui et al., 2023). Nanofluidic systems made of other 2D or 1D materials, such as hexagonal boron nitride (hBN), MoS_2, black phosphorus (BP), and boron nitride nanotubes (BNNTs), have also been developed. These systems exhibited a surface charge density of -0.12, -0.3, -4, and -1000 to -100 mC m^{-2}, respectively (Siria et al., 2013; Esfandiar et al., 2017; Cui et al., 2023).

Polyethylene terephthalate (PET) is another popular material for fabricating nanofluidic systems. The track-etch method, which uses accelerated heavy ions to hit and etch a substrate, has been widely used to create PET nanochannels or nanopores (Siwy et al., 2003). The PET surfaces under this fabrication method are usually negatively charged due to intrinsic carboxylate groups on the surfaces. The surface charge density covers a wide range, from -240 mC m^{-2} (Siwy et al., 2005) to -10 mC m^{-2} (Xue et al., 2009). Such a large range is caused by various fabrication parameters, such as post-bombard etchant concentration and etching time.

Membrane-based nanofluidic systems using the phenomenon of nanoscale capillary effects have also been used to study the surface charge effects. Graphene oxide (GO) nanosheet membranes show relatively weak surface charge densities (-20.1 to -0.12 mC m^{-2}) (Hong et al., 2017). However, high surface charge densities can be reached in boron nitride (BN) membrane (-840 mC m^{-2}) (Qin et al., 2017). MXene $Ti_3C_2T_x$ membranes and metal-organic framework (MOF) UiO-66-COOH membranes can be fabricated with surface charge densities ranging from -800 to -100 mC m^{-2} (Hong et al., 2019; Lu et al., 2021).

In addition to negatively charged surfaces, some materials can carry positive charges, such as Al_2O_3, MgO, and NiO. Al_2O_3 layers can be grown by electron-beam (e-beam) evaporation or thermal atomic layer deposition (ALD). E-beam evaporation is usually performed in a high vacuum chamber, which usually results in a lower surface charge density. Thermal ALD is performed in a relatively high-pressure chamber, where there is certain oxygen and the surface may contain a high charge density. MgO layers can only be grown by e-beam evaporation and NiO layers can be created using e-beam evaporation of Ni and a subsequent oxidation process. The positive charge sites on these oxide surfaces originate from the protonate process of the surface chemical equilibrium, i.e., $\text{-MO} + H^+ \leftrightharpoons \text{-MOH}^+$, where -MO represents the surface oxide group. The surface charge densities of these materials may vary from ~2.0 to ~4.0 mC m^{-2} (Cheng, 2008; Cheng and Guo, 2009).

2.2 Surface charge tuning by surface modifications

Surface charge polarity and density can also be regulated through surface chemical modifications. Table 2 summarizes some surface chemical modification methods. For SiO_2-base materials, such as fused silica and lead-rich glass, several modification methods have been developed for tuning the surface charge density. One strategy is to block the surface charges on pristine surfaces by attaching the surface with neutral chemical groups. Octodecyltrichlorosilane (OTS) modification for fused silica surface is an example. OTS treatment allows OTS molecules to form a self-assembled monolayer, which can hinder the surface charges.

TABLE 2 Surface charge polarity and density achieved by surface modifications.

Modification method	Substrate	Polarity	Charge density (mC m^{-2})	Refs.
OTS treatment	Fused silica	Negative	−21 and −10.8	Stein et al. (2004)
3-aminopropyldimethyl-ethoxy silane acetonitrile solution treatment	Glass nanopore	Positive	-	Wang et al. (2006)
Polymer poly-L-lysine (PLL) treatment	Fused silica	Positive	-	Stein et al. (2004)
1st step: 1-(3-Dimethylaminopropyl)-3-ethylcarbodiimide (EDC); 2nd step: 1-aminopropyl-3-methylimidazolium bromide (APMIB)	GO membrane	Positive	147	Ji et al. (2017)
Layer-by-layer deposition of polyelectrolytes	Track-etched PET nanopores	Negative or positive	−6.4 to 144	Ali et al. (2010)
EDC solution treatment	Track-etched PET conical nanopores	Positive	-	Vlassiouk and Siwy (2007)
Succinic anhydride solution treatment	Track-etched PET conical nanopores	Negative	-	Vlassiouk and Siwy (2007)
Cetyl trimethyl ammonium bromide (CTAB) treatment	Track-etched PET nanopores	Negative or positive	−9 to 8	Xie et al. (2009)
1. Etched in a water-reactive environment inside an SEM	Graphite	Negative	−2000 to −340	Emmerich et al. (2022)
2. Etched in O_2 using RIE				
Oxygen plasma treatment	Graphene nanopore	Negative	−240	Shan et al. (2013)
Oxygen plasma treatment	PMMA nanoslit	Negative	−38.2	Uba et al. (2015)
Oxygen plasma treatment	PMMA nanochannel	Negative	−40.5	Uba et al. (2015)
Amine treatment	PMMA nanoslit	Positive	28.4	Uba et al. (2015)
Amine treatment	PMMA nanochannel	Positive	22.9	Uba et al. (2015)

Since the CH_3 head groups of the OTS monolayer do not carry any surface charges, the modified fused silica surface shows a weak surface charge density. The coverage of OTS molecules can be tuned by adjusting the duration of modification or the modification solution concentration. Different OTS molecule coverages make the modified surface exhibit various surface charge densities. Stein et al. reported that the surface charge density of fused silica could be changed from −60 to −10.8 mC m^{-2} through OTS treatments (Stein et al., 2004).

The second strategy is by introducing charged functional groups. 3-aminopropyldimethyl-ethoxy silane acetonitrile solution treatment can attach -NH_2 groups to lead-rich glass capillaries. In electrolyte solutions with a low pH value, the -NH_2 groups attached on the surface experience a protonation process, becoming positively charged -NH_3^+ groups. Thus, the modified surface carries positive charges (Wang et al., 2006; Liu et al., 2012). Polymer poly-L-lysine (PLL) treatment can also achieve the same goal as well. PLL treatment adds -NH_2 groups to the fused silica surface and the -NH_2 groups protonate at a low pH value, resulting in positively charged -NH_3^+ groups. Therefore, the modified surface is positively charged (Stein et al., 2004). This universal strategy can be applied to other materials. Ji et al. developed a two-step scheme to fabricate positively charged GO membranes, where carbodiimide was created on the GO membrane in the first step and 1-aminopropyl-3-methylimidazolium bromide (APMIB) was conjugated subsequently. The APMIB was positively charged, which caused the GO membrane to carry positive charges (Ji et al., 2017).

For PET nanopores, several chemical modification methods have been proposed to control the surface charge density, including layer-by-layer deposition of polyelectrolytes (Ali et al., 2010), 1-(3-Dimethylaminopropyl)-3-ethylcarbodiimide (EDC) solution treatment (Vlassiouk and Siwy, 2007), succinic anhydride solution treatment (Vlassiouk and Siwy, 2007), and cetyl trimethyl ammonium bromide (CTAB) treatment (Xie et al., 2009). Layer-by-layer deposition of polyelectrolytes first deposits poly-(allylamine hydrochloride) (PAH) molecules to PET nanopores through electrostatic adsorption. Because PET nanopores carry anionic carboxylate groups and PAH molecules have many positively charged -NH_3^+ groups, the resulting assemblies provide excessive positively charged -NH_3^+ groups, which make the modified surface positively charged. Upon the positively charged PET surface, poly (styrenesulfonate) (PSS) treatment can be applied to reverse the surface polarity. PSS molecules have abundant negatively charged -SO_3^- groups and they electrostatically assemble to -NH_3^+ groups. This leads to a -SO_3^--group-terminated surface, which is negatively charged. EDC solution treatment aminates PET nanopore surfaces and the resulted -NH_3^+ groups make the surface positively charged. The PET nanopore surfaces bonding with -NH_3^+ can be transformed back to carboxylate-group-terminated surfaces by succinic anhydride

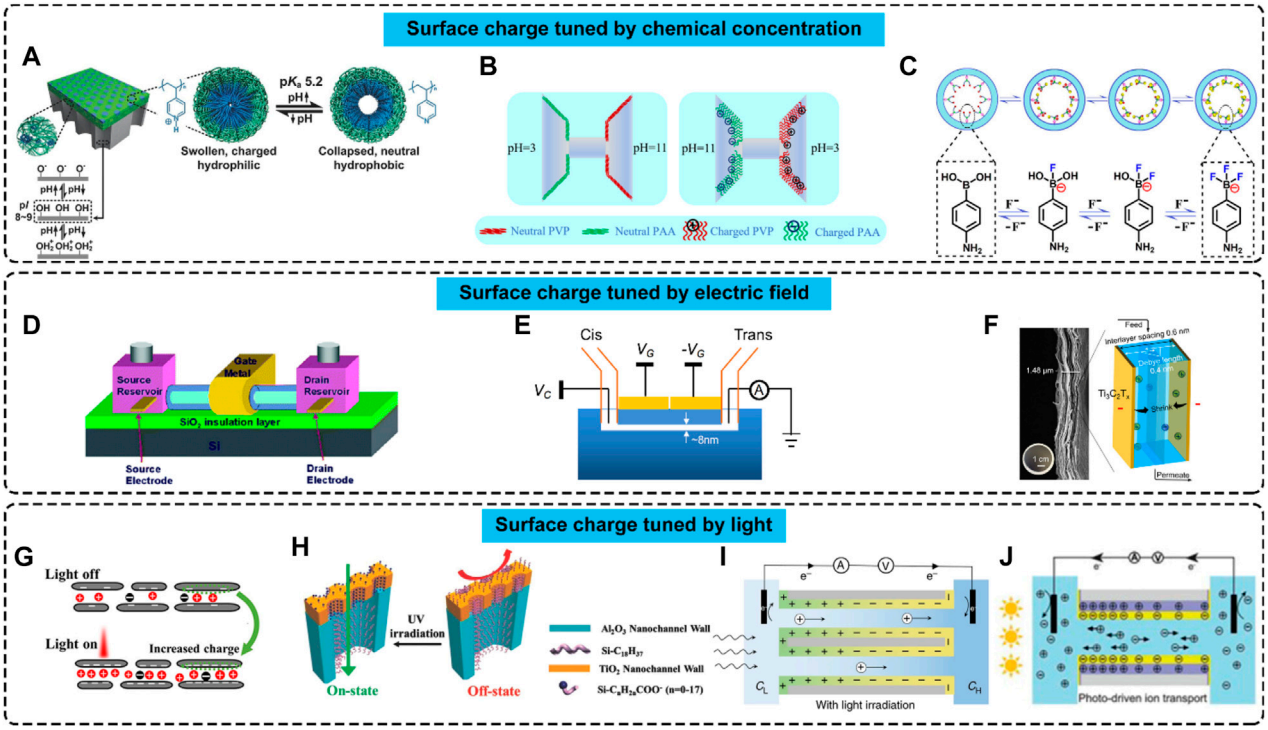

FIGURE 2
Nanofluidic systems with surface charges tuned by external fields. **(A–C)** Surface charge tuned by chemical concentrations. From left to right: Adapted with permission (Zhang et al., 2016). Copyright 2015, John Wiley and Sons. Adapted with permission (Li et al., 2022). Copyright 2022, American Chemical Society. Adapted with permission (Liu et al., 2014). Copyright 2014, American Chemical Society. **(D–F)** Surface charge changed by electric fields. From left to right: Adapted with permission (Karnik et al., 2005). Copyright 2005, American Chemical Society. Adapted with permission (Ren et al., 2018). Copyright 2018, American Chemical Society. **(G–J)** Surface charges regulated by light. From left to right: Adapted with permission (Su et al., 2021). Copyright 2021, American Chemical Society. Adapted with permission (Zhang et al., 2014). Copyright 2013, John Wiley and Sons. Copyright 2019, Nature Publishing Group. Copyright 2020, Oxford University Press.

solution treatment, which exhibit negatively charged. The modification method using cetyl trimethyl ammonium bromide (CTAB) can make the surface charge density of PET nanopores chemical concentration-dependent. When PET nanopores are modified by a low-concentration CTAB solution, cetyltrimethylammonium ions (CTA^+) are absorbed onto the pore surface due to strong electrostatic effects and the surface is mildly charged. When the CTAB solution concentration is increased, more CTA^+ groups attach onto the surface, changing the surface from a negatively charged state to a neutral state. If the CTAB solution concentration becomes sufficiently high, CTA^+ groups accumulate on the surface, which can reverse the surface polarity and cause the surface to be positively charged.

Surface modifications under a gaseous environment have been reported as well. Emmerich et al. developed an activation method for graphite. The first step was to etch the graphite in a water-reactive environment inside a scanning electron microscope (SEM) chamber, and the second step was to etch it in an oxygen (O_2) plasma environment in a reactive ion etching (RIE) chamber. Graphite with extremely strong surface charge densities from −2000 to −340 mC m^{-2} were achieved using this approach. The activation phenomenon for these two configurations were explained by highly reactive radicals and crystalline structure defects (Emmerich et al., 2022). Oxygen plasma treatment is also feasible for graphene nanopores (Shan et al., 2013) and PMMA nanofluidic systems (Uba et al., 2015).

2.3 Surface charge tuning by external fields

The surface charge polarity and density can also be modified by various external fields. Figure 2 illustrates three methods. The first method is through altering chemical concentrations. Changing the concentration of H^+, or pH value, is one of the most common and effective approaches. Zhang et al. reported that porous anodic alumina membrane's surface charge polarity and density varied under pH stimuli, as shown in Figure 2A. The porous anodic alumina surface experienced a protonation process and gradually exhibited neutral and then positively charged characteristics when the pH value of the electrolyte solution was decreased. When the pH value was increased, a deprotonation process occurred, and the surface became neutral, then negatively charged from a positively charged state (Zhang et al., 2016). It has also been shown that Poly (acrylic acid) (PAA) and poly (4-vinylpyridine) (PVP) can be employed for polydimethylsiloxane (PDMS) nanochannels to achieve a similar pH-responsive surface charge density. Figure 2B shows such a case containing PDMS channels. When pH=3, the PAA-coated PDMS surface was neutral. However, the PVP-coated PDMS surface was positively charged. At pH=11, the PAA-coated

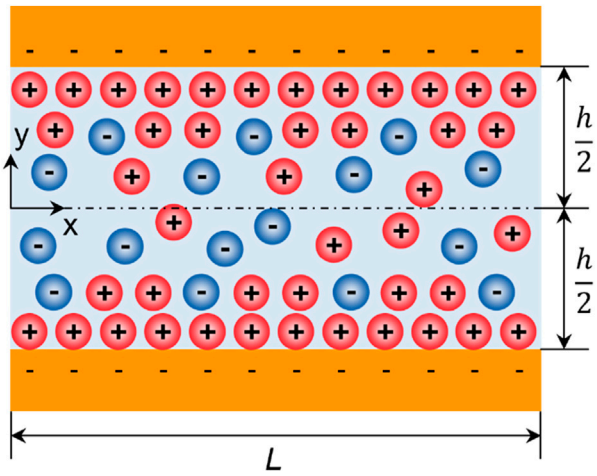

FIGURE 3
Schematic and notations for a nanochannel for ionic conductance analysis.

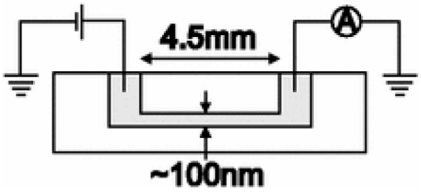

FIGURE 4
Experimental setup for ionic conductance measurement. It contains a slit-like nanochannel, a power supply, and a current meter. Reprinted with permission (Stein et al., 2004). Copyright 2004, American Physical Society.

surface became negatively charged, while the PVP-coated surface was neutral (Li et al., 2022). Figure 2C depicts another concentration-responsive scheme for changing the surface charge properties, i.e., through adjusting the concentration of fluoride. Upon the increase of fluoride concentration in the solution, 4-aminophenylboronic-acid (APBA) molecules on the modified nanochannels experienced a transformation from a neutral state to negatively charged monofluoride adducts ($RB(OH)_2F^-$), difluoride adducts ($RB(OH)F_2^-$), and trifluoride adducts (RBF_3^-). Meanwhile, the transformation was reversible, i.e., the modified surface could resume the neutral state upon reducing the fluoride concentration (Liu et al., 2014).

The second method uses external electric fields. Karnik et al. demonstrated a nanofluidic transistor consisting of a source reservoir, a drain reservoir, a gate metal coating, and a nanotube or several parallel nanochannels, as shown in Figure 2D. Analogous to electronic metal-oxide-field-effect-transistors (MOSFETs), where the electronic current can be tuned by a gate voltage, the nanofluidic transistor enabled the control of ionic currents by electric gating. This phenomenon was caused by the charge density variance induced by the external electric field and surface charge-governed ionic flows. Quantitative investigations showed that the achievable surface charge density ranged from −100 to −2 mC m^{-2} for parallel nanochannels and from −20 to −10 mC m^{-2} for nanotubes (Karnik et al., 2005). Guan et al. developed a nanofluidic system, which contained two electric gates above nanochannels, as shown in Figure 2E. With this electric gate arrangement, gating voltages in opposite polarities were applied to different parts of the nanochannels simultaneously. Hence, the nanochannels simultaneously owned positively and negatively charged regions, resulting in diverse functions (Guan, 2013). Figure 2F illustrates the case, where an electric gate was applied to MXene $Ti_3C_2T_x$ membranes. The ion permeation in this case was enhanced, indicating that the surface charge densities of the membranes were increased.

The third way to tune surface charge is using light. Su et al. observed that the ionic conductivity of MoS_2 membranes could be enhanced under the illumination of UV light, which was caused by the light-enhanced surface charge density (Su et al., 2021), as demonstrated in Figure 2G. Zhang et al. reported a fabrication method to make membranes with heterogeneous surface charge distribution through TiO_2-assisted photochemical reactions. As shown in Figure 2H, TiO_2/Al_2O_3 heterogeneous nanochannels were coated with OTS molecules before light modification. Then, UV irradiation was applied to the as-prepared nanochannels, which caused the OTS molecules on the TiO_2 surface to decompose, and eventually carboxylic groups were created on the surface, making the surface negatively charged. In contrast, the OTS molecules on the Al_2O_3 surface remained unchanged. This resulted in heterogenous surface charge properties. In this strategy, the decomposition reactions of OTS molecules were irreversible. Therefore, the surface charge distribution would not change after the removal of UV irradiation (Zhang et al., 2014). Reversible surface charge tuning is achievable by using photo-responsive materials, such as semiconductors or semiconductor heterojunctions. Kai et al. proposed a photo-driven ion pump using a semiconducting carbon nitride nanotube membrane. Under light illumination, photo-induced holes moved to the illuminated side and photo-induced electrons moved to the unilluminated side, resulting in an asymmetrical charge distribution, as shown in Figure 2I. The photo-induced charge gradient caused a surface charge density gradient on the nanochannel wall. Once the light irradiation was removed, the photo-induced charge separation disappeared and the uneven surface charge distribution vanished (Xiao et al., 2019). A similar idea was applied to TiO_2/C_3N_4 heterojunction nanotubes, as shown in Figure 2J, where the as-fabricated nanofluidic system had a surface charge gradient on the nanochannel wall (Xiao et al., 2021).

3 Surface charge characterizations

3.1 Estimated by ionic conductance

A theory describing ion transport in nanochannels has been developed by Stein et al. (Stein et al., 2004). The theory divides the transport problem into two scenarios, based on the quantitative relationship between the Debye screening length, κ^{-1} ($\kappa^2 = \frac{2e^2n}{\varepsilon\varepsilon_0 k_B T}$) and the channel height, h. If the notations for a nanochannel in Figure 3 are used, for the first scenario, at high ion concentrations, where $\kappa h \gg 1$ and the surface charge density, σ, is small,

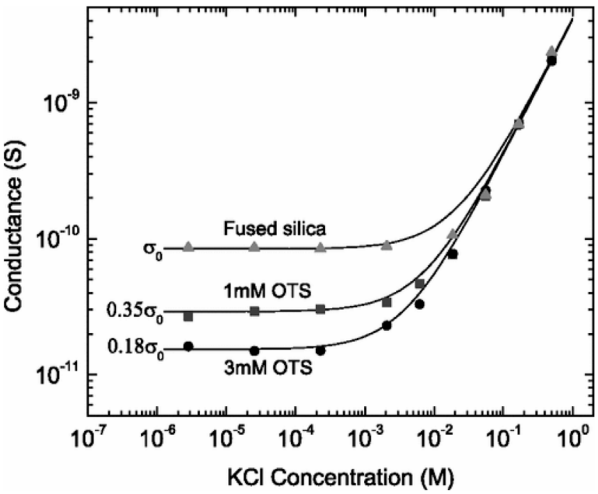

FIGURE 5
Ionic conductance as a function of KCl concentration in fused silica nanoslit fluidic systems. The data can be used to estimate the surface charge density, σ, of the untreated fused silica channels and channels modified by 1 mM and 3 mM OTS. Reprinted with permission (Stein et al., 2004). Copyright 2004, American Physical Society.

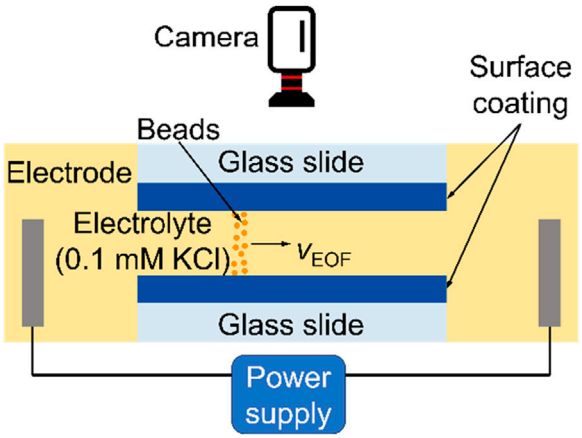

FIGURE 6
An experimental setup for electroosmotic flow measurement.

i.e., $|\sigma| \ll enh$, where e is the elementary charge and n is the number density of ions, the ionic conductance, G, is approximately given by (Li, 2018)

$$G \approx \frac{2ne\mu hw}{L} \tag{1}$$

where μ is the bulk mobility of ions, w, and L are the channel width and length, respectively (see Figure 3). Eq. 1 shows that the ionic conductance directly depends on the ion concentration and channel dimensions and appears to be independent of the surface charge density, which is consistent with the classic model.

At low ion concentrations, however, the surface charge plays an important role in affecting G. In this case, $\kappa h \ll 1$ and $|\sigma| \gg enh$, and G is given by

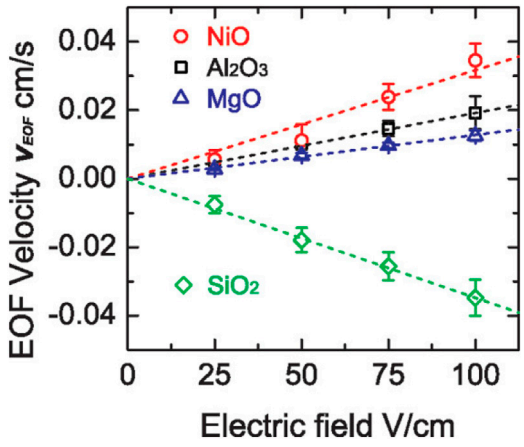

FIGURE 7
Electroosmotic flow velocity as a function of electric field for different surface coatings. Adapted with permission (Cheng and Guo, 2009). Copyright 2009, American Chemical Society.

$$G \approx |\sigma| \frac{\mu w}{L}\left(1 + \frac{4\varepsilon\varepsilon_0 k_B T}{e\mu\eta}\right) \tag{2}$$

where ε is the dielectric constant of water, ε_0 is the permittivity of free space, k_B is the Boltzmann constant, T is temperature, and η is the fluid viscosity. Eq. 2 indicates that G is independent of the ion concentration, but strongly depends on σ.

Eq. 2 provides a practical protocol for estimating σ of a nanofluidic system. For an experimental setup illustrated in Figure 4, G can be obtained based on the ionic current measured and the voltage applied. By changing the electrolyte concentration, a relationship between G and the ion concentration of the electrolyte is determined. G at the low ion concentration limit (e.g., 10^{-6}–10^{-4} M) can be used to predict σ using Eq. 2. To ensure the accuracy of σ estimation, the measurements of G can be repeated by altering the nanochannel height from tens of nanometers to hundreds of nanometers.

An example is depicted in Figure 5, where fused silica nanoslit channels were modified by 1 mM and 3 mM OTS solutions. σ was determined using Eq. 2. It was found that σ for the surfaces treated by 1 mM and 3 mM OTS solutions was reduced by 35% and 18% compared with the untreated channels, respectively (Stein et al., 2004).

3.2 Electroosmotic flow method

The surface charge density σ can also be assessed using electroosmotic flows. For a nanofluidic system containing nanoslit channels, if fluid properties are assumed to be uniform and under the stick boundary condition, the electroosmotic flow velocity, V_{EOF}, should increase linearly with increasing electric field, E, applied to the system. According to the Smoluchowski equation, V_{EOF} is given as

$$V_{EOF} = -\left(\frac{\varepsilon\varepsilon_0\varsigma}{\eta}\right)E \tag{3}$$

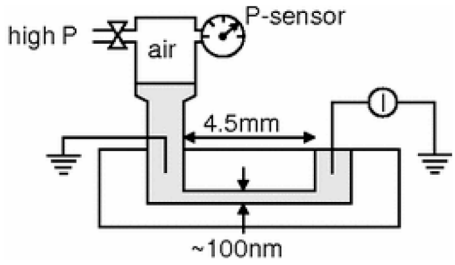

FIGURE 8
Schematic of a nanofluidic system for I_{str} measurement. Reprinted with permission (van der Heyden et al., 2005). Copyright 2005, American Physical Society.

where ζ is the zeta-potential. If the channel height is relatively large, it can be assumed that ζ is approximately equal to the surface potential ψ_s. Then, σ can be estimated by the Grahame equation

$$\sigma = \sqrt{8\varepsilon\varepsilon_0 k_B T n}\, sinh\left(\frac{q\psi_s}{2k_B T}\right) \tag{4}$$

where n is the number density of ions.

Figure 6 shows an experiment setup to determine σ by analyzing the data obtained from electroosmotic flow measurements, which was reported by (Cheng and Guo, 2009; Cheng, 2008.). The experimental system comprised a microfluidic chamber, two electrodes, a power supply, and a camera. The microfluidic chamber consisted of two pieces of glass slides coated with films of interest. The height, width, and length of the microchannel were 80 μm, 0.5 cm, and 1 cm, respectively. An electrolyte (0.1 mM KCl solution) and 1-μm diameter polystyrene beads, which were used to display the flow velocity, were filled into the chamber. Figure 7 plots V_{EOF} as a function of the electric field for various coatings. The slope of the data points equals to $-\varepsilon\varepsilon_0\varsigma/\eta$, which was used to calculate σ. By this method, the surface charge densities of SiO_2, Al_2O_3, MgO, and NiO were determined as −4.24, 2.10, 1.36, and 3.77 mC m^{-2}, respectively.

3.3 Estimation based on streaming currents

The surface charge density σ can also be determined using the streaming current of a nanofluidic system. A theory describing the streaming current (I_{str}) in a single nanochannel has been developed by (van der Heyden et al., 2005). Figure 8 depicts an experimental setup for measuring the streaming current. It consisted of a nanochannel, a pressure chamber, where high-pressure air was used to change the fluid pressure inside the channel, a pressure sensor (P-sensor), and an ammeter for measuring the streaming current through the nanochannel. With this setup, a relationship between the streaming current I_{str} and the applied pressure difference ΔP, can be obtained. The streaming conductance, S_{str}, is then calculated as

$$S_{str} = \frac{dI_{str}}{d\Delta P} \tag{5}$$

where, with the notations in Figure 3, I_{str}, is calculated as

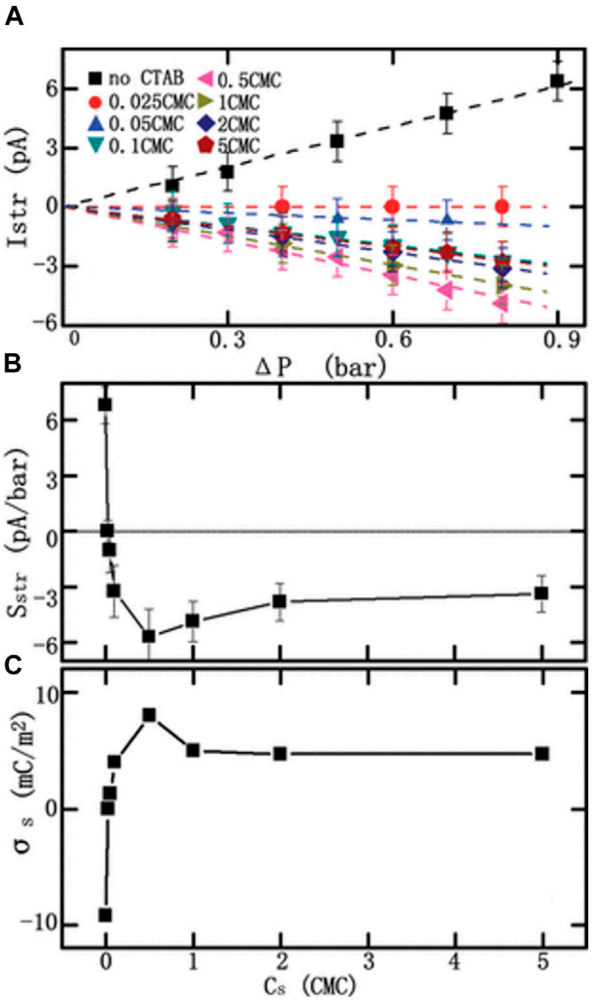

FIGURE 9
Theoretical estimation of surface charge density, σ, by measuring the streaming current, I_{str}. **(A)** I_{str} as a function of pressure difference, ΔP. **(B)** Streaming conductance S_{str} as a function of the modification concentration, C_s. **(C)** σ as a function of C_s. Adapted with permission (Xie et al., 2009). Copyright 2009, American Chemical Society.

$$I_{str} = w\int_{-\frac{h}{2}}^{\frac{h}{2}} \rho_e(y)u(y)dy \tag{6}$$

where ρ_e is the ion density. It is given by Poisson's equation,

$$\rho_e(y) = -\frac{\varepsilon\varepsilon_0 k_B T}{e}\cdot\frac{d^2\psi(y)}{dy^2} \tag{7}$$

where the electrical potential $\psi(y)$ is described by the Poisson-Boltzmann equation,

$$\frac{d^2\psi(y)}{dy^2} = \frac{k_B T\kappa^2}{e} sinh\left(\frac{e\psi(y)}{k_B T}\right) \tag{8}$$

The analytical solution of Eq. 8 gives $\psi(y)$,

$$\psi(y) = \psi_0 + \frac{2k_B T}{e} ln(\mathrm{JacCD}(z\,|\,m)) \tag{9}$$

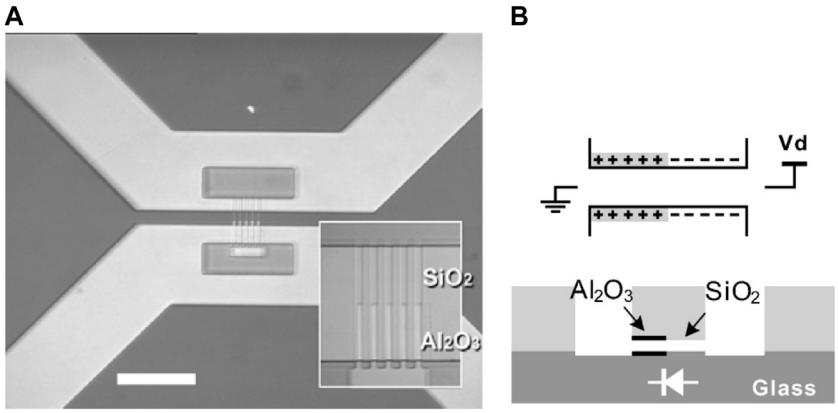

FIGURE 10
A nanoscale ionic diode. **(A)** SEM image of the fluidic system with asymmetric surface charges due to heterogeneous coatings. **(B)** Schematic of the charge distribution and nanochannel structure. Adapted with permission (Cheng and Guo, 2009). Copyright 2009, American Chemical Society.

where ψ_0 is the potential at the centerline of the channel and JacCD $(z|m)$ is the Jacobi elliptic function ($z = \frac{\kappa y}{2} e^{-e\psi_0/2k_BT}$ and $m = e^{2e\psi_0/k_BT}$). To obtain ψ_0, a boundary condition regarding σ is employed by Gauss's law,

$$\sigma = \pm \varepsilon\varepsilon_0 E_e\left(x = \mp\frac{h}{2}\right) \tag{10}$$

where the electric field, $E_e(y)$, is given by

$$E_e(y) = -\frac{d\psi(y)}{dy} \tag{11}$$

The velocity distribution $u(y)$ in Eq. 6 is given by Poiseuille's law,

$$u(y) = \frac{\Delta P}{8L\eta}(h^2 - 4y^2) \tag{12}$$

Plug Eqs 7, 12 into Eq. 6, it is obtained that

$$I_{str} = -\frac{w\Delta P}{8L\eta}\int_{-\frac{h}{2}}^{\frac{h}{2}} \rho_e(y)\cdot(h^2 - 4y^2)dy \tag{13}$$

Then, S_{str} reads

$$S_{str} = -\frac{w}{8L\eta}\int_{-\frac{h}{2}}^{\frac{h}{2}} \rho_e(y)\cdot(h^2 - 4y^2)dy \tag{14}$$

Equations 6–14 show that S_{Str} is related to σ, which can be estimated based on the value of S_{Str}. Details regarding the determination of σ using the streaming current can be found in the literature (van der Heyden et al., 2005; van der Heyden et al., 2006; van der Heyden et al., 2007). An example of this method is shown in Figure 9, where σ of modified PET nanopores was obtained (Xie et al., 2009). In this work, S_{str} for the flow through the PET nanopores was measured. The method employed CTAB solutions with different concentrations, which enabled different molecular assemblies attached onto the modified nanopore surfaces and caused the surface to carry different charges. I_{str} was measured under various pressure drops (Figure 9A). The slopes of the I_{str}-ΔP curves were obtained as S_{str}, which is plotted *versus* the CTAB solution concentration in Figure 9B. Eventually, σ for the nanopores was calculated as a function of the CTAB solutions, as shown in Figure 9C.

3.4 Estimation using functional groups

For surfaces modified by functional groups, the surface charge polarity can be estimated based on the structure and polarity of the functional groups. Ji et al. fabricated a negatively charged GO membrane by assembling carboxylic acid groups on the surface (Ji et al., 2017). X-ray photoelectron spectroscopy was employed to determine the density of surface functional group of the as-prepared surface, indicating that carboxylic acid group took up ~2.0% of the total carbon content on the membrane surface. Then, the surface charge density was calculated by multiplying the density and the charges of the functional groups, which showed a result of −123 mC m^{-2}. This method has also been applied to determine the surface charge density of MOF-based membranes (Lu et al., 2021) and chemical-modified PET nanopores (Ali et al., 2010).

4 Applications

4.1 Nanofluidic ionic diodes

Various nanofluidic ionic diodes have been developed and reported in the literature. The concept of nanofluidic ionic diodes is analogous to electronic semiconductor diodes. A nanofluidic ionic diode allows ion transport in a favorable direction when a forward bias is applied (open state) while hindering the ion migration in the opposite direction when a backward bias is applied (close form). The underlying mechanism is the appearance of an ion depletion region, which is similar to the charge depletion region in a semiconductor p-n junction diode. Under a forward bias, the depletion region does not appear inside the nanochannel, and the transport of ions is allowed. Under a backward bias, the depletion region is created, where the ion concentration is low. Ions can hardly move across the depletion region. The key to achieving the ion depletion region under a

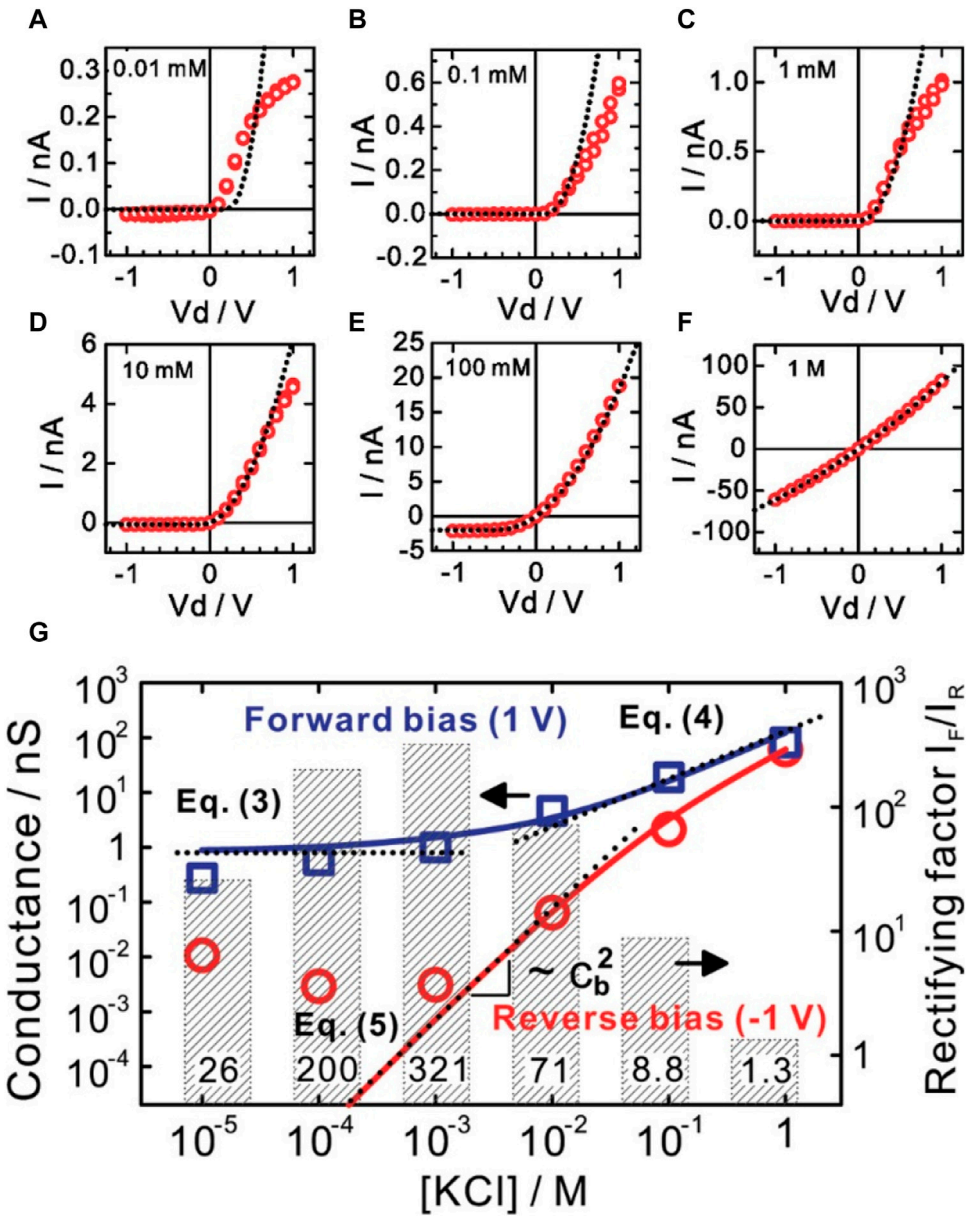

FIGURE 11
Performance of the ionic diode shown in Figure 10. **(A–F)** *I-V* curves at various concentrations. **(G)** Ionic conductance and rectification factor as a function of KCl concentration. Adapted with permission (Cheng and Guo, 2009). Copyright 2009, American Chemical Society.

backward bias is asymmetry, either in geometry or surface charge distribution. Cheng et al. proposed an ionic diode by creating counter-charged regions in a nanochannel array (Cheng and Guo, 2009). An SEM image of the diode is shown in Figure 10A and the structure of the diode is schematically depicted in Figure 10B. For the nanochannels, half of the surfaces were coated with Al_2O_3, which was positively charged, while the other half was coated with SiO_2, which was negatively charged. Figure 11 summarizes the device's performance with electrolytes of different concentrations. When a negative bias was applied at low concentrations (0.01–100 mM), the ionic current did not change and remained low. However, when a positive bias was imposed, the ionic current increased with increasing bias. The rectification factor, which is the ratio of the ionic currents under the forward and the backward bias, reached the maximum value of 321. The synergy effect of the highly charged surface and asymmetric geometry caused the enhancement of the rectification factor and improved the performance of the diode. A numerical study by Pal Singh et al. revealed that a high surface charge density increases the electrolyte's unipolar character in a bipolar nanochannel-based fluidic diode. Specifically, the ion depletion was enhanced and the ion current decreased when a backward bias was applied, which resulted in a promoted ion current rectification (Pal Singh et al., 2011). Moreover, a more significant current rectification effect could be generated by combining geometry asymmetry and surface charge asymmetry, as reported by Xiao et al. (Xiao

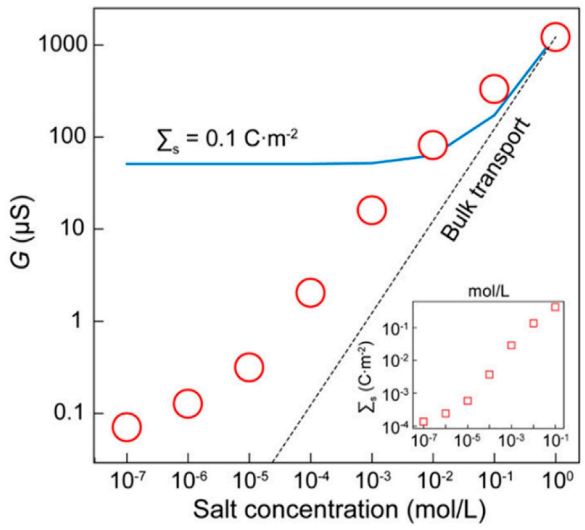

FIGURE 12
Ionic conductance of MXene membranes (red circles) as a function of salt concentration. The dashed line represents the case of neutral membranes. The solid line represents the predictions for a constant surface charge density of 0.1 mC m^{-2}. The inset shows the surface charge density as a function of salt concentration. Adapted with permission (Hong et al., 2019). Copyright 2019, American Chemical Society.

et al., 2016), where untreated funnel-shaped nanochannels with a uniform surface charge distribution were employed and the highest rectification ratio was about 13.5. For the treated funnel-shaped nanochannels with surface charge asymmetry, i.e., the conical segment of the funnel was positively charged and the cylindrical segment of the funnel was negatively charged, the rectification ratio reached 553. The enhanced ionic rectification was due to the accumulation and depletion of ions at the cylindrical segment, which was caused by the asymmetric surface charges.

4.2 Osmotic power generator

Nanofluidic osmotic power generators are devices that convert the energy from cation or anion flows through nanochannels/pores into electrical energy. Such a device usually consists of two chambers separated by an array of nanochannels or a thin membrane with nanoscale pores. One chamber contains a salt solution with a high concentration, while the other one is filled with a low-concentration solution. When the two solutions are brought into contact, the salinity gradient drives the ions to migrate from the high concentration end to the low concentration end. Due to the sieving effect of the charged nanochannels/pores, only ions with specific charges (either cations or anions) can pass through, which creates an osmotic voltage and osmotic current across the two chambers. The sieving effect of the nanochannels/pores depends on the surface charge. Therefore, the surface charge density plays a critical role in osmotic power generation. Numerous studies have been conducted to improve the conversion efficiency of osmotic power generators by enhancing the surface charge density of the nanochannels/pores. Hong et al. reported an osmotic power harvesting system using MXene $Ti_3C_2T_x$ membranes (Hong et al., 2019). The ionic conductance, *G*, of the system as a function of the salt concentration is shown in Figure 12. It is seen that *G* is higher than that for the system containing neutral membranes. The enhancement was caused by the highly charged MXene membrane surfaces.

Regulating counter-ion transport from the high salinity chamber to the low salinity chamber by counter-charged nanochannels is another way to achieve high electrical outputs. Gao et al. developed and fabricated a heterogenous membrane with positively charged pores on one side and negatively charged pores on the other side

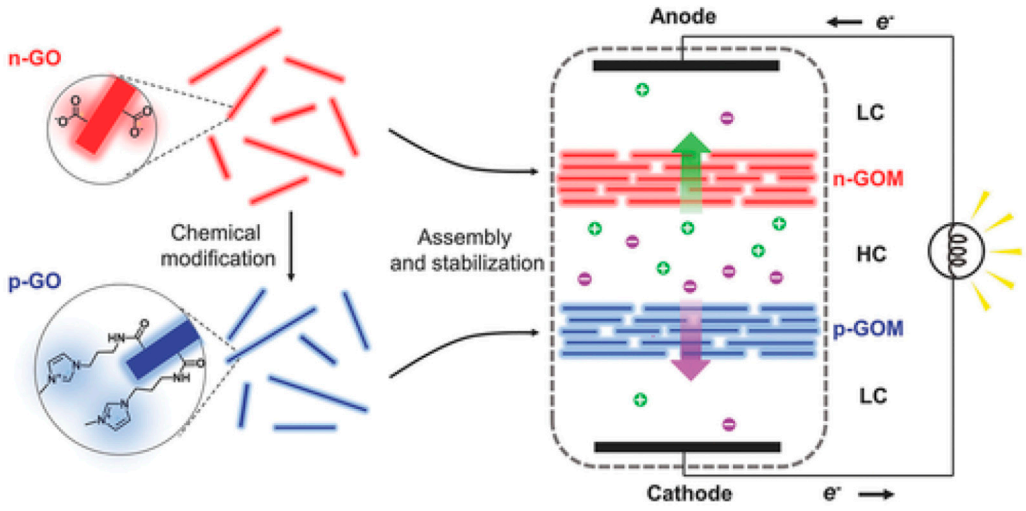

FIGURE 13
An osmotic power generator with a pair of positively and negatively charged graphene oxide membranes. Adapted with permission (Ji et al., 2017). Copyright 2016, John Wiley and Sons.

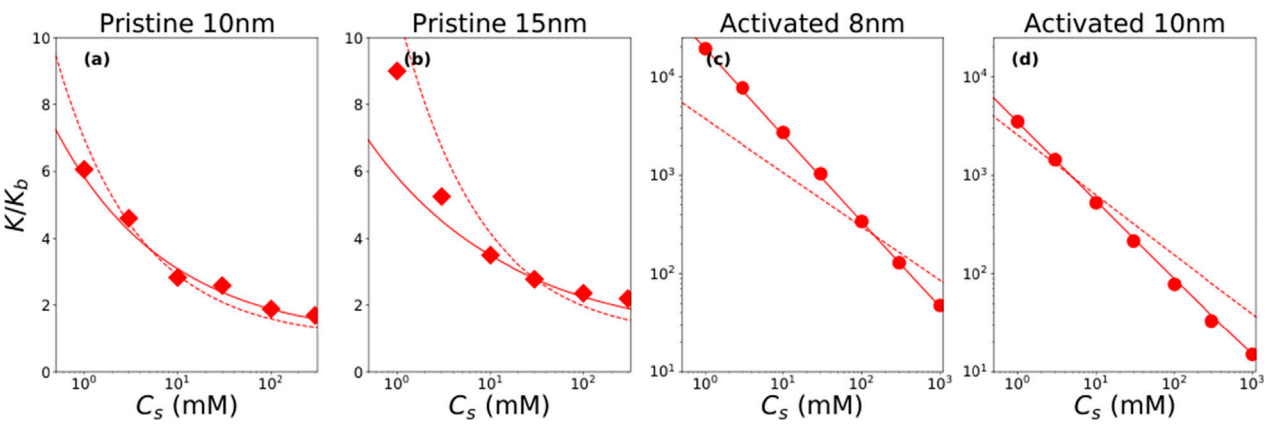

FIGURE 14
Conductivity enhancement for pristine and activated nanochannels at different concentrations (Emmerich, 2021). **(A)** Pristine nanochannel with a height of 10 nm. **(B)** Pristine nanochannel with a height of 15 nm. **(C)** Activated nanochannel with a height of 8 nm. **(D)** Activated nanochannel with a height of 10 nm. Symbols represent experimental data. Solid and dashed lines are theoretical predictions with different assumptions.

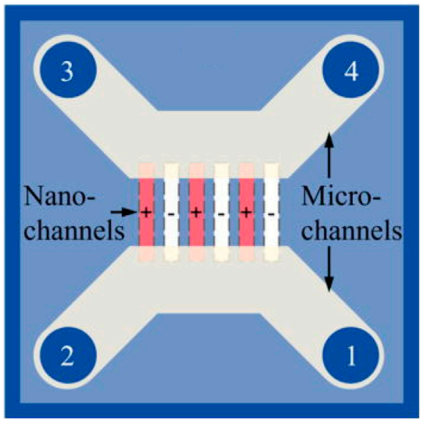

FIGURE 15
Schematic of a nanofluidic system with counter-charged nanochannels. Reprinted with the permission of AIP Publishing (Zhou et al., 2023).

(Gao et al., 2023). The positively charged pores were achieved by an ordered alumina nanochannel membrane (ANM), which had a surface charge density of 7.18 mC m^{-2} and a pore size of 100 nm. The negatively charged pores were achieved by the β-ketoenamine-linked two-dimensional covalent-organic framework (COF) membrane with a surface charge density of −5.14 mC m^{-2} and a pore size of 1.1 nm. The proposed heterogeneous membrane reached an osmotic power density of 27.8 W m^{-2} when salt gradient was created by artificial salt-lake and river water. Similar heterogenous membranes with positively and negatively charged pores for power generation have been reported by several groups as well (Zhou et al., 2021; Cao et al., 2022; Fauziah et al., 2023; Wang et al., 2023). Ji et al. reported an osmotic power generator with a pair of positively and negatively charged GO membranes, as shown in Figure 13 (Ji et al., 2017). It achieved an output power density of 0.77 W m^{-2} when artificial seawater and river water were added to the high and low salinity sides, respectively. The configuration with positively and negatively charged membranes can be achieved by stacking positively and negatively charged nanoparticles as well (Wang et al., 2018). The positively charged membranes were fabricated by packing aminated silica-coated iron oxide nanoparticles and negatively charged ones were fabricated by hydroxyl-group-bonded silica and polystyrene nanoparticles. Each full cell consisted of a positively charged membrane and a negatively charged membrane. When 20 full cells were connected in series, the device achieved an output voltage as high as 1 V.

4.3 Ion transport enhancement

Ion transport in nanochannels can be enhanced by changing the surface charge density. Several studies have demonstrated superior ionic conductance in highly charged nanochannels. As shown in Figure 14, Emmerich et al. demonstrated that the ionic conductance in activated nanochannels could be enhanced by 10,000 times compared with the bulk value. They attributed such a significant improvement to one to two orders of magnitude increase in the surface charge density during the activation process (Emmerich, 2021). Fast ion transport was also observed in nanochannels consisting of mica and graphite, as reported by Jiang et al. (2023). The mica surface showed a very high surface charge density, which was around −200 mC m^{-2}. This highly charged mica surface absorbed a large number of cations, forming a cation stack with a packing density close to the 2D dense packing limit. The highly packed cation stack migrated under an electric field, which demonstrated an ionic conductivity orders of magnitude higher than the bulk value.

Recently, a new strategy for enhancing ion transport in nanofluidic systems was proposed by using counter-charged nanochannels, where half of the nanochannels were positively charged and the other half of the nanochannels were negatively charged (Zhou et al., 2023). Figure 15 illustrates the design of the system. Positively charged nanochannels were achieved by coating surface with Al_2O_3 and negatively charged nanochannels were pristine SiO_2. In such a fluidic system, cations and anions moved

in different channels, which avoided opposite-directional migration of ions in the same channel under an electric field and boosted the velocity of ions. Numerical simulations showed that the ionic current could be enhanced by a factor up to 5.8 at a proper surface charge density. In experiments, the maximum current was 1.8 times the bulk value, which is lower than numerical results due to a relatively low surface charge density.

5 Summary and outlook

In conclusion, we have reviewed the recent progress in nanofluidic systems with tunable surface charges for ion transport. Surface fabrications, surface charge characterizations, and applications are discussed. For surface fabrications, pristine surfaces and surface charge properties under various fabrication methods in the literature are summarized. Furthermore, various surface modification methods that can be used to tune surface charge polarity or density by chemical solutions or in gaseous environments are introduced. External fields including chemical concentration, electric field, and light for altering the surface charge density are also discussed. Materials, techniques, and underlying mechanisms for surface charge modifications are elaborated.

Primary methods for surface charge characterizations are presented in the second part. Theoretical estimations can be performed using ionic conductance, electroosmotic flows, streaming currents, and the density of functional groups. Necessary theories for characterization analysis are described. Experimental setups and nanofluidic system configurations involved in these characterization methods are provided. Examples from the literature are presented for reference.

The third part of this review deals with the applications of surface charge-dominated ion transport in nanofluidic systems. Three major applications are discussed. Nanofluidic ionic diodes, which take advantage of asymmetric geometry and/or surface charge distribution of nanochannels, allow ion transport in a particular direction and suppress the ionic current in the reverse direction. Osmotic power generators convert energy of osmotic flows to electricity. Their efficiency can be enhanced by increasing the surface charge density or regulating ionic flows through oppositely charged membranes. Counter-charged nanochannels can be utilized to boost ion transport in nanofluidic systems and the ionic current enhancement can be adjusted by varying the surface charged density.

For future developments, several issues need to be investigated and addressed. First, various pristine surfaces show negative charges, but few carry positive charges. More efforts can be made to explore the possibility of making pristine surfaces positively charged. This will provide flexibility for nanofluidic system fabrication in terms of material selection. Second, regarding the surface charge tuned by external fields, nanochannels with surface charges being tuned through a joint method (e.g., tuned simultaneously by an electric field and light) can be studied, which may shed light on more powerful nanofluidic systems. Third, the results about surface charge characterizations in the literature are based on different methods. It is difficult to compare them. It would be convenient for data comparison if a standard protocol for surface charge characterizations can be developed.

Regarding the potential applications, topics such as nanofluidic memristors and nanofluidic membranes for salt-lake lithium mining can be considered. Nanofluidic memristors are a type of memory resistors achieved in nanofluidic systems that have an internal state which can be altered based on the voltage history of the system, resulting in a change in their conductance (Robin et al., 2023). If nanofluidic systems with voltage-responsive hysteretic surface charge can be developed, nanofluidic memristors facilitating this mechanism can be achieved. Salt-lake lithium mining is proposed as a solution to meet the increasing demand for lithium ions in battery industry. The surface charge properties of nanofluidic membranes are of great importance in this application, as they can control the behavior of Li^+ inside nanopores (Razmjou et al., 2019; Hou et al., 2021). However, limited surface charge tuning techniques have hindered the progress in this area. With the advances in nanofluidic systems with tunable surface charges, the selective transport of Li^+ is expected to be enhanced.

Author contributions

DS: Conceptualization, Data curation, Formal Analysis, Writing–original draft. LZ: Conceptualization, Data curation, Formal Analysis, Writing–original draft. ZL: Conceptualization, Funding acquisition, Project administration, Supervision, Writing–review and editing.

Funding

The author(s) declare financial support was received for the research, authorship, and/or publication of this article. This work was supported by the General Research Fund (16208422 and 16207323) and Collaborative Research Fund (C6020-22G) of the Hong Kong Special Administrative Region.

Conflict of interest

The authors declare that the research was conducted in the absence of any commercial or financial relationships that could be construed as a potential conflict of interest.

Publisher's note

References

Ali, M., Yameen, B., Cervera, J., Ramírez, P., Neumann, R., Ensinger, W., et al. (2010). Layer-by-Layer assembly of polyelectrolytes into ionic current rectifying solid-state nanopores: insights from theory and experiment. *J. Am. Chem. Soc.* 132, 8338–8348. doi:10.1021/ja101014y

Bakli, C., and Chakraborty, S. (2015). Electrokinetic energy conversion in nanofluidic channels: addressing the loose ends in nanodevice efficiency. *ELECTROPHORESIS* 36, 675–681. doi:10.1002/elps.201400317

Bocquet, L., and Charlaix, E. (2010). Nanofluidics, from bulk to interfaces. *Chem. Soc. Rev.* 39, 1073–1095. doi:10.1039/B909366B

Cao, L., Chen, I.-C., Liu, X., Li, Z., Zhou, Z., and Lai, Z. (2022). An ionic diode covalent organic framework membrane for efficient osmotic energy conversion. *ACS Nano* 16, 18910–18920. doi:10.1021/acsnano.2c07813

Chen, Z., Wang, Y., Wang, W., and Li, Z. (2009). Nanofluidic electrokinetics in nanoparticle crystal. *Appl. Phys. Lett.* 95, 102105. doi:10.1063/1.3223774

Cheng, L.-J. (2008). *Ion and molecule transport in nanochannels*. Ann Arbor, Michigan: The University of Michigan.

Cheng, L.-J., and Guo, L. J. (2009). Ionic current rectification, breakdown, and switching in heterogeneous oxide nanofluidic devices. *ACS Nano* 3, 575–584. doi:10.1021/nn8007542

Cui, G., Xu, Z., Li, H., Zhang, S., Xu, L., Siria, A., et al. (2023a). Enhanced osmotic transport in individual double-walled carbon nanotube. *Nat. Commun.* 14, 2295. doi:10.1038/s41467-023-37970-3

Cui, Y., Guo, H., Yan, X., Zhou, W., Ye, Q., Ying, C., et al. (2023b). Nonlinear and anisotropic ion transport in black phosphorus nanochannels. *Nano Lett.* 23, 5886–5893. doi:10.1021/acs.nanolett.3c00078

Daiguji, H. (2010). Ion transport in nanofluidic channels. *Chem. Soc. Rev.* 39, 901–911. doi:10.1039/B820556F

Daiguji, H., Oka, Y., Adachi, T., and Shirono, K. (2006). Theoretical study on the efficiency of nanofluidic batteries. *Electrochem. Commun.* 8, 1796–1800. doi:10.1016/j.elecom.2006.08.003

Daiguji, H., Oka, Y., and Shirono, K. (2005). Nanofluidic diode and bipolar transistor. *Nano Lett.* 5, 2274–2280. doi:10.1021/nl051646y

Emmerich, T. (2021). *Activated carbon nanofluidics: from blue energy to ionic memory*. Paris: École normale supérieure.

Emmerich, T., Vasu, K. S., Niguès, A., Keerthi, A., Radha, B., Siria, A., et al. (2022). Enhanced nanofluidic transport in activated carbon nanoconduits. *Nat. Mat.* 21, 696–702. doi:10.1038/s41563-022-01229-x

Esfandiar, A., Radha, B., Wang, F. C., Yang, Q., Hu, S., Garaj, S., et al. (2017). Size effect in ion transport through angstrom-scale slits. *Science* 358, 511–513. doi:10.1126/science.aan5275

Fan, R., Yue, M., Karnik, R., Majumdar, A., and Yang, P. (2005). Polarity switching and transient responses in single nanotube nanofluidic transistors. *Phys. Rev. Lett.* 95, 086607. doi:10.1103/PhysRevLett.95.086607

Fauziah, A. R., Chu, C.-W., and Yeh, L.-H. (2023). Engineered subnanochannel ionic diode membranes based on metal–organic frameworks for boosted lithium ion transport and osmotic energy conversion in organic solution. *Chem. Eng. J.* 452, 139244. doi:10.1016/j.cej.2022.139244

Fu, J., Schoch, R. B., Stevens, A. L., Tannenbaum, S. R., and Han, J. (2007). A patterned anisotropic nanofluidic sieving structure for continuous-flow separation of DNA and proteins. *Nat. Nanotech* 2, 121–128. doi:10.1038/nnano.2006.206

Fuest, M., Rangharajan, K. K., Boone, C., Conlisk, A. T., and Prakash, S. (2017). Cation dependent surface charge regulation in gated nanofluidic devices. *Anal. Chem.* 89, 1593–1601. doi:10.1021/acs.analchem.6b03653

Gao, J., Liu, X., Jiang, Y., Ding, L., Jiang, L., and Guo, W. (2019). Understanding the giant gap between single-pore- and membrane-based nanofluidic osmotic power generators. *Small* 15, 1804279. doi:10.1002/smll.201804279

Gao, M., Zheng, M.-J., El-Mahdy, A. F. M., Chang, C.-W., Su, Y.-C., Hung, W.-H., et al. (2023). A bioinspired ionic diode membrane based on sub-2 nm covalent organic framework channels for ultrahigh osmotic energy generation. *Nano Energy* 105, 108007. doi:10.1016/j.nanoen.2022.108007

Guan, W. (2013). *Electrofluidics in micro/nanofluidic systems*. Yale University.

Han, W., and Chen, X. (2020). A review: applications of ion transport in micro-nanofluidic systems based on ion concentration polarization. *J. Chem. Technol. Biotechnol.* 95, 1622–1631. doi:10.1002/jctb.6288

Hong, S., Constans, C., Surmani Martins, M. V., Seow, Y. C., Guevara Carrió, J. A., and Garaj, S. (2017). Scalable graphene-based membranes for ionic sieving with ultrahigh charge selectivity. *Nano Lett.* 17, 728–732. doi:10.1021/acs.nanolett.6b03837

Hong, S., Ming, F., Shi, Y., Li, R., Kim, I. S., Tang, C. Y., et al. (2019). Two-dimensional $Ti_3C_2T_{<i>x</i>}$ MXene membranes as nanofluidic osmotic power generators. *ACS Nano* 13, 8917–8925. doi:10.1021/acsnano.9b02579

Hou, L., Xian, W., Bing, S., Song, Y., Sun, Q., Zhang, L., et al. (2021). Understanding the ion transport behavior across nanofluidic membranes in response to the charge variations. *Adv. Funct. Mater.* 31, 2009970. doi:10.1002/adfm.202009970

Ji, J., Kang, Q., Zhou, Y., Feng, Y., Chen, X., Yuan, J., et al. (2017). Osmotic power generation with positively and negatively charged 2D nanofluidic membrane pairs. *Adv. Funct. Mater.* 27, 1603623. doi:10.1002/adfm.201603623

Jia, Z., Choi, J., Lee, S., Soper, S. A., and Park, S. (2022). Modifying surface charge density of thermoplastic nanofluidic biosensors by multivalent cations within the slip plane of the electric double layer. *Colloids Surfaces A Physicochem. Eng. Aspects* 648, 129147. doi:10.1016/j.colsurfa.2022.129147

Jiang, Y., Hu, R., Yang, C., Zhou, Z., Yuan, G., Zhou, H., et al. (2023). Surface diffusion enhanced ion transport through two-dimensional nanochannels. *Sci. Adv.* 9, eadi8493. doi:10.1126/sciadv.adi8493

Jin, Y., Ng, T., Tao, R., Luo, S., Su, Y., and Li, Z. (2020). Coupling effects in electromechanical ion transport in graphene nanochannels. *Phys. Rev. E* 102, 033112. doi:10.1103/PhysRevE.102.033112

Kang, S., Mathwig, K., and Lemay, S. G. (2012). Response time of nanofluidic electrochemical sensors. *Lab a Chip* 12, 1262–1267. doi:10.1039/C2LC21104A

Karnik, R., Duan, C., Castelino, K., Daiguji, H., and Majumdar, A. (2007). Rectification of ionic current in a nanofluidic diode. *Nano Lett.* 7, 547–551. doi:10.1021/nl062806o

Karnik, R., Fan, R., Yue, M., Li, D., Yang, P., and Majumdar, A. (2005). Electrostatic control of ions and molecules in nanofluidic transistors. *Nano Lett.* 5, 943–948. doi:10.1021/nl050493b

Lebedev, D., Malyshev, G., Ryzhkov, I., Mozharov, A., Shugurov, K., Sharov, V., et al. (2021). Focused ion beam milling based formation of nanochannels in silicon-glass microfluidic chips for the study of ion transport. *Microfluid Nanofluid* 25, 51. doi:10.1007/s10404-021-02450-x

Li, D. (2022). *Electrokinetic microfluidics and nanofluidics*. Springer Nature.

Li, J., Zhang, K., Zhao, X., and Li, D. (2022). Single artificial ion channels with tunable ion transport based on the surface modification of pH-responsive polymers. *ACS Appl. Mat. Interfaces* 14, 27130–27139. doi:10.1021/acsami.2c03949

Li, T., Li, S. X., Kong, W., Chen, C., Hitz, E., Jia, C., et al. (2019). A nanofluidic ion regulation membrane with aligned cellulose nanofibers. *Sci. Adv.* 5, eaau4238. doi:10.1126/sciadv.aau4238

Li, Y., Tu, L., Ma, X., Chen, H., Fan, Y., Zhou, Q., et al. (2021). Engineering a smart nanofluidic sensor for high-performance peroxynitrite sensing through a spirocyclic ring open/close reaction strategy. *ACS Sens.* 6, 808–814. doi:10.1021/acssensors.0c01719

Li, Z. (2018). *Nanofluidics: an introduction*. Boca Raton: CRC Press.

Liu, B., Zhou, L., Luo, S., Zhou, Y., Yang, J., and Li, Z. (2022). Diffusion coefficient of ions through graphene nanopores. *AIP Adv.* 12, 085227. doi:10.1063/5.0098641

Liu, J., Kvetny, M., Feng, J., Wang, D., Wu, B., Brown, W., et al. (2012). Surface charge density determination of single conical nanopores based on normalized ion current rectification. *Langmuir* 28, 1588–1595. doi:10.1021/la203106w

Liu, Q., Xiao, K., Wen, L., Dong, Y., Xie, G., Zhang, Z., et al. (2014). A fluoride-driven ionic gate based on a 4-aminophenylboronic acid-functionalized asymmetric single nanochannel. *ACS Nano* 8, 12292–12299. doi:10.1021/nn506257c

Lu, J., Zhang, H., Hu, X., Qian, B., Hou, J., Han, L., et al. (2021). Ultraselective monovalent metal ion conduction in a three-dimensional sub-1 nm nanofluidic device constructed by metal–organic frameworks. *ACS Nano* 15, 1240–1249. doi:10.1021/acsnano.0c08328

Ma, Y., Su, Y.-S., Qian, S., and Yeh, L.-H. (2017). Analytical model for surface-charge-governed nanochannel conductance. *Sensors Actuators B Chem.* 247, 697–705. doi:10.1016/j.snb.2017.03.080

Miedema, H., Vrouenraets, M., Wierenga, J., Meijberg, W., Robillard, G., and Eisenberg, B. (2007). A biological porin engineered into a molecular, nanofluidic diode. *Nano Lett.* 7, 2886–2891. doi:10.1021/nl0716808

Napoli, M., Eijkel, T., Pennathur, S., and Pennathur, S. (2010). Nanofluidic technology for biomolecule applications: a critical review. *Lab a Chip* 10, 957–985. doi:10.1039/B917759K

Ouyang, W., Wang, W., Zhang, H., Wu, W., and Li, Z. (2013). Nanofluidic crystal: a facile, high-efficiency and high-power-density scaling up scheme for energy harvesting based on nanofluidic reverse electrodialysis. *Nanotechnology* 24, 345401. doi:10.1088/0957-4484/24/34/345401

Pal Singh, K., Kumari, K., and Kumar, M. (2011). Ion current rectification in a fluidic bipolar nanochannel with smooth junction. *Appl. Phys. Lett.* 99, 113103. doi:10.1063/1.3627181

Pan, Y., Zhou, Y., Zhao, Q., Dou, Y., Chou, S., Cheng, F., et al. (2017). Introducing ion-transport-regulating nanochannels to lithium-sulfur batteries. *Nano Energy* 33, 205–212. doi:10.1016/j.nanoen.2017.01.025

Pang, P., He, J., Park, J. H., Krstić, P. S., and Lindsay, S. (2011). Origin of giant ionic currents in carbon nanotube channels. *ACS Nano* 5, 7277–7283. doi:10.1021/nn202115s

Qian, S., and Xuan, X. (2020). Editorial for the special issue on micro/nano-chip electrokinetics, Vol. III. *Micromachines* 11, 482. doi:10.3390/mi11050482

Qin, S., Liu, D., Wang, G., Portehault, D., Garvey, C. J., Gogotsi, Y., et al. (2017). High and stable ionic conductivity in 2D nanofluidic ion channels between boron nitride layers. *J. Am. Chem. Soc.* 139, 6314–6320. doi:10.1021/jacs.6b11100

Rauscher, M., and Dietrich, S. (2008). Wetting phenomena in nanofluidics. *Annu. Rev. Mater. Res.* 38, 143–172. doi:10.1146/annurev.matsci.38.060407.132451

Razmjou, A., Asadnia, M., Hosseini, E., Habibnejad Korayem, A., and Chen, V. (2019). Design principles of ion selective nanostructured membranes for the extraction of lithium ions. *Nat. Commun.* 10, 5793. doi:10.1038/s41467-019-13648-7

Rems, L., Kawale, D., Lee, L. J., and Boukany, P. E. (2016). Flow of DNA in micro/nanofluidics: from fundamentals to applications. *Biomicrofluidics* 10, 043403. doi:10.1063/1.4958719

Ren, C. E., Alhabeb, M., Byles, B. W., Zhao, M.-Q., Anasori, B., Pomerantseva, E., et al. (2018). Voltage-gated ions sieving through 2D MXene $Ti_3C_2T_{<i>x</i>}$ membranes. *ACS Appl. Nano Mat.* 1, 3644–3652. doi:10.1021/acsanm.8b00762

Robin, P., Emmerich, T., Ismail, A., Niguès, A., You, Y., Nam, G.-H., et al. (2023). Long-term memory and synapse-like dynamics in two-dimensional nanofluidic channels. *Science* 379, 161–167. doi:10.1126/science.adc9931

Sang, J., Du, H., Wang, W., Chu, M., Wang, Y., Li, H., et al. (2013). Protein sensing by nanofluidic crystal and its signal enhancement. *Biomicrofluidics* 7, 024112. doi:10.1063/1.4802936

Schoch, R. B., Han, J., and Renaud, P. (2008). Transport phenomena in nanofluidics. *Rev. Mod. Phys.* 80, 839–883. doi:10.1103/RevModPhys.80.839

Schoch, R. B., and Renaud, P. (2005). Ion transport through nanoslits dominated by the effective surface charge. *Appl. Phys. Lett.* 86, 253111. doi:10.1063/1.1954899

Shan, Y. P., Tiwari, P. B., Krishnakumar, P., Vlassiouk, I., Li, W. Z., Wang, X. W., et al. (2013). Surface modification of graphene nanopores for protein translocation. *Nanotechnology* 24, 495102. doi:10.1088/0957-4484/24/49/495102

Si, L., Wu, Y., Xiao, H., Xing, W., Song, R., Li, Y., et al. (2023). A superstable, flexible, and scalable nanofluidic ion regulation composite membrane. *Sci. Bull.* 68, 2344–2353. doi:10.1016/j.scib.2023.08.060

Siria, A., Poncharal, P., Biance, A.-L., Fulcrand, R., Blase, X., Purcell, S. T., et al. (2013). Giant osmotic energy conversion measured in a single transmembrane boron nitride nanotube. *Nature* 494, 455–458. doi:10.1038/nature11876

Siwy, Z., Apel, P., Baur, D., Dobrev, D. D., Korchev, Y. E., Neumann, R., et al. (2003). Preparation of synthetic nanopores with transport properties analogous to biological channels. *Surf. Sci.* 532-535 (535), 1061–1066. doi:10.1016/S0039-6028(03)00448-5

Siwy, Z., Kosińska, I. D., Fuliński, A., and Martin, C. R. (2005). Asymmetric diffusion through synthetic nanopores. *Phys. Rev. Lett.* 94, 048102. doi:10.1103/PhysRevLett.94.048102

Stein, D., Kruithof, M., and Dekker, C. (2004). Surface-charge-governed ion transport in nanofluidic channels. *Phys. Rev. Lett.* 93, 035901. doi:10.1103/PhysRevLett.93.035901

Su, Y., Liu, D., Yang, G., Wang, L., Razal, J. M., and Lei, W. (2021). Light-controlled ionic transport through molybdenum disulfide membranes. *ACS Appl. Mat. Interfaces* 13, 34679–34685. doi:10.1021/acsami.1c04698

Tao, R., Gao, X., Lin, D., Chen, Y., Jin, Y., Chen, X., et al. (2021). The role of entrance functionalization in carbon nanotube-based nanofluidic systems: an intrinsic challenge. *Phys. Fluids* 33, 012015. doi:10.1063/5.0037208

Timperman, A. (2019). Joshua edel, aleksandar ivanov, MinJun kim (eds.): nanofluidics, 2nd ed. *Anal. Bioanal. Chem.* 411, 1299–1300. doi:10.1007/s00216-019-01585-9

Uba, I., Pullagurla, S. R., Sirasunthorn, N., Wu, J., Park, S., Chantiwas, R., et al. (2015). Surface charge, electroosmotic flow and DNA extension in chemically modified thermoplastic nanoslits and nanochannels. *Analyst* 140, 113–126. doi:10.1039/C4AN01439A

Utko, P., Persson, F., Kristensen, A., and Larsen, N. B. (2011). Injection molded nanofluidic chips: fabrication method and functional tests using single-molecule DNA experiments. *Lab. Chip* 11, 303–308. doi:10.1039/C0LC00260G

van der Heyden, F. H. J., Bonthuis, D. J., Stein, D., Meyer, C., and Dekker, C. (2006). Electrokinetic energy conversion efficiency in nanofluidic channels. *Nano Lett.* 6, 2232–2237. doi:10.1021/nl061524l

van der Heyden, F. H. J., Bonthuis, D. J., Stein, D., Meyer, C., and Dekker, C. (2007). Power generation by pressure-driven transport of ions in nanofluidic channels. *Nano Lett.* 7, 1022–1025. doi:10.1021/nl070194h

van der Heyden, F. H. J., Stein, D., and Dekker, C. (2005). Streaming currents in a single nanofluidic channel. *Phys. Rev. Lett.* 95, 116104. doi:10.1103/PhysRevLett.95.116104

Vlassiouk, I., Kozel, T. R., and Siwy, Z. S. (2009). Biosensing with nanofluidic diodes. *J. Am. Chem. Soc.* 131, 8211–8220. doi:10.1021/ja901120f

Vlassiouk, I., and Siwy, Z. S. (2007). Nanofluidic diode. *Nano Lett.* 7, 552–556. doi:10.1021/nl062924b

Vlassiouk, I., Smirnov, S., and Siwy, Z. (2008). Ionic selectivity of single nanochannels. *Nano Lett.* 8, 1978–1985. doi:10.1021/nl800949k

Wang, C., Choi, E., and Park, J. (2018). High-voltage nanofluidic energy generator based on ion-concentration-gradients mimicking electric eels. *Nano Energy* 43, 291–299. doi:10.1016/j.nanoen.2017.11.054

Wang, G., Zhang, B., Wayment, J. R., Harris, J. M., and White, H. S. (2006). Electrostatic-gated transport in chemically modified glass nanopore electrodes. *J. Am. Chem. Soc.* 128, 7679–7686. doi:10.1021/ja061357r

Wang, J., Wang, L., Shao, N., He, M., Shang, P., Cui, Z., et al. (2023). Heterogeneous Two-dimensional lamellar Ti3C2Tx membrane for osmotic power harvesting. *Chem. Eng. J.* 452, 139531. doi:10.1016/j.cej.2022.139531

Wang, L., and Chen, Y. (2022). Bioinspired dual-driven binary heterogeneous nanofluidic ionic diodes. *Langmuir* 38, 12450–12456. doi:10.1021/acs.langmuir.2c01570

Xiao, K., Chen, L., Chen, R., Heil, T., Lemus, S. D. C., Fan, F., et al. (2019). Artificial light-driven ion pump for photoelectric energy conversion. *Nat. Commun.* 10, 74. doi:10.1038/s41467-018-08029-5

Xiao, K., Giusto, P., Chen, F., Chen, R., Heil, T., Cao, S., et al. (2021). Light-driven directional ion transport for enhanced osmotic energy harvesting. *Natl. Sci. Rev.* 8, nwaa231. doi:10.1093/nsr/nwaa231

Xiao, K., Giusto, P., Wen, L., Jiang, L., and Antonietti, M. (2018). Nanofluidic ion transport and energy conversion through ultrathin free-standing polymeric carbon nitride membranes. *Angew. Chem. Int. Ed.* 57, 10123–10126. doi:10.1002/anie.201804299

Xiao, K., Xie, G., Zhang, Z., Kong, X.-Y., Liu, Q., Li, P., et al. (2016). Enhanced stability and controllability of an ionic diode based on funnel-shaped nanochannels with an extended critical region. *Adv. Mater.* 28, 3345–3350. doi:10.1002/adma.201505842

Xie, Q., Alibakhshi, M. A., Jiao, S., Xu, Z., Hempel, M., Kong, J., et al. (2018). Fast water transport in graphene nanofluidic channels. *Nat. Nanotech* 13, 238–245. doi:10.1038/s41565-017-0031-9

Xie, Q., Xin, F., Park, H. G., and Duan, C. (2016). Ion transport in graphene nanofluidic channels. *Nanoscale* 8, 19527–19535. doi:10.1039/C6NR06977K

Xie, Y., Xue, J., Wang, L., Wang, X., Jin, K., Chen, L., et al. (2009). Surface modification of single track-etched nanopores with surfactant CTAB. *Langmuir* 25, 8870–8874. doi:10.1021/la9017213

Xue, J., Xie, Y., Yan, Y., Ke, J., and Wang, Y. (2009). Surface charge density of the track-etched nanopores in polyethylene terephthalate foils. *Biomicrofluidics* 3, 022408. doi:10.1063/1.3130988

Yan, C., Lv, C., Zhu, Y., Chen, G., Sun, J., and Yu, G. (2017). Engineering 2D nanofluidic Li-ion transport channels for superior electrochemical energy storage. *Adv. Mater.* 29, 1703909. doi:10.1002/adma.201703909

Yeh, L.-H., Zhang, M., and Qian, S. (2013). Ion transport in a pH-regulated nanopore. *Anal. Chem.* 85, 7527–7534. doi:10.1021/ac401536g

Zhang, M., Sheng, N., Song, Q., Zhang, H., Chen, S., Wang, H., et al. (2022). Enhanced selective ion transport by assembling nanofibers to membrane pairs with channel-like nanopores for osmotic energy harvesting. *Nano Energy* 103, 107786. doi:10.1016/j.nanoen.2022.107786

Zhang, Q., Hu, Z., Liu, Z., Zhai, J., and Jiang, L. (2014). Light-gating titania/alumina heterogeneous nanochannels with regulatable ion rectification characteristic. *Adv. Funct. Mater.* 24, 424–431. doi:10.1002/adfm.201301426

Zhang, Z., Kong, X.-Y., Xiao, K., Xie, G., Liu, Q., Tian, Y., et al. (2016). A bioinspired multifunctional heterogeneous membrane with ultrahigh ionic rectification and highly efficient selective ionic gating. *Adv. Mater.* 28, 144–150. doi:10.1002/adma.201503668

Zhao, W., Wang, B., and Wang, W. (2016). Biochemical sensing by nanofluidic crystal in a confined space. *Lab a Chip* 16, 2050–2058. doi:10.1039/C6LC00416D

Zhou, K., Kovarik, M. L., and Jacobson, S. C. (2008). Surface-charge induced ion depletion and sample stacking near single nanopores in microfluidic devices. *J. Am. Chem. Soc.* 130, 8614–8616. doi:10.1021/ja802692x

Zhou, K., Perry, J. M., and Jacobson, S. C. (2011). Transport and sensing in nanofluidic devices. *Annu. Rev. Anal. Chem.* 4, 321–341. doi:10.1146/annurev-anchem-061010-113938

Zhou, L., Shi, D., Lin, S., Zhou, Y., and Li, Z. (2023). Enhancing ion transport in nanofluidic systems through counter-charged nanochannels. *Phys. Fluids* 35, 092001. doi:10.1063/5.0167203

Zhou, S., Xie, L., Li, X., Huang, Y., Zhang, L., Liang, Q., et al. (2021). Interfacial super-assembly of ordered mesoporous carbon-silica/AAO hybrid membrane with enhanced permselectivity for temperature- and pH-sensitive smart ion transport. *Angew. Chem. Int. Ed.* 60, 26167–26176. doi:10.1002/anie.202110731

Zhou, Y., Ding, H., Smith, A. T., Jia, X., Chen, S., Liu, L., et al. (2019). Nanofluidic energy conversion and molecular separation through highly stable clay-based membranes. *J. Mater. Chem. A* 7, 14089–14096. doi:10.1039/C9TA00801B